11

Dusty plasmas

MIHÁLY HORÁNYI

11.1 Motivation

The study of dusty plasmas bridges a number of traditionally separate subjects, for example, celestial mechanics, mechanics of granular materials, and plasma physics. Dust particles, typically micron- and submicron-sized solid objects, immersed in plasmas and UV radiation collect electrostatic charges and respond to electromagnetic forces in addition to all the other forces acting on uncharged grains. Simultaneously, dust can alter its plasma environment by acting as a possible sink and/or source of electrons and ions. Dust particles in plasmas are unusual charge carriers. They are many orders of magnitude heavier than any other plasma particles, and they can have many orders of magnitude larger (negative or positive) time-dependent charges. Dust particles can communicate non-electromagnetic effects, including gravity, neutral gas and plasma drag, and radiation pressure to the plasma electrons and ions. Their presence can influence the collective plasma behavior by altering the traditional plasma wave modes and by triggering new types of waves and instabilities. Dusty plasmas represent the most general form of space, laboratory, and industrial plasmas. Interplanetary space, comets, planetary rings, asteroids, the Moon, and aerosols in the atmosphere, are all examples where electrons, ions, and dust particles coexist.

The observations of the inward transport of interstellar dust and the outflow of near-solar dust provide a unique opportunity to explore dusty plasma processes throughout the heliosphere. The flux, direction, and size distribution of interstellar dust can be used to test our models about the large-scale structure of the heliospheric magnetic fields, and its temporal variability with solar cycle. The measurements of the speed, composition, and size distribution of the recently discovered, solar-wind-entrained, nano-dust particles hold the key to understanding their effects on the dynamics and composition of the solar-wind plasma.

After its fly-by of Jupiter, the dust detector onboard the Ulysses spacecraft detected impacts of particles in the mass range of 10^{-14} to 10^{-11} g, predominantly

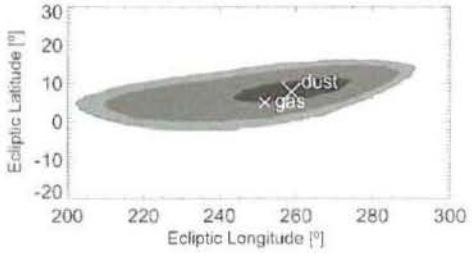

Fig. 11.1 The upstream direction of the interstellar dust flux observed by Ulysses is $\lambda = 259 \pm 20°$ and $\theta = 8 \pm 10°$ ecliptic longitude and latitude, respectively. The contour plot shows 1, 2, and 3 σ confidence levels as black, dark gray, and light gray. The helium upstream direction is $\lambda = 254°, \theta = 5.6°$. (From Frisch *et al.*, 1999.)

from a direction that was opposite to the expected impact direction of interplanetary dust grains. In addition, the impact velocities exceeded the local solar-system escape velocity (Grün *et al.*, 1993). Subsequent analysis showed that the motion of the interstellar grains through the solar system was approximately parallel to the flow of neutral interstellar hydrogen and helium gas (Fig. 11.1), both traveling at a speed of 26 km/s. The 20-year-long journey of these small dust particles through the heliosphere is strongly coupled to the large-scale structure of the heliospheric magnetic fields (IMF) through almost two full solar cycles. Hence, monitoring the variability of the flux of interstellar dust (ISD) grains provides a unique opportunity to test our models of the IMF through solar cycles (Sterken *et al.*, 2013).

The interaction of dust particles with the heliospheric magnetic fields depends on the grain's mass, charge, and material properties. The smallest interstellar grains (radii <10 nm) remain tied to the interstellar magnetic fields and are diverted around the heliosphere (Frisch *et al.*, 1999), only larger grains can penetrate the heliosphere. The Lorentz force created by the solar-wind magnetic field sweeping past the grains can both repel or focus the grains, depending on the configuration of the field and thus on the phase of the solar cycle (Grün *et al.*, 1994). In mid 1996, the flux of ISD grains was observed to decrease by a factor 3 as a result of the electromagnetic interaction of the grains with the magnetic field of the solar wind (Landgraf, 2000). The polarity of this magnetic field changes with the 22-year solar cycle. During the solar maximum in 1991, the field polarity became north-pointing. The azimuthal component of the expanding magnetic field deflected interstellar grains in the northern hemisphere to the north and grains in the southern hemisphere to the south. Thus, the net effect of the interplanetary magnetic field during the 1991 polarity cycle was to divert interstellar dust away from the ecliptic plane. During the 2000/2001 solar maximum the field polarity reversed. However, interstellar grains need about 20 years (almost 2 solar cycles) to

traverse the distance from the heliospheric boundary (at about 100 AU) to the Sun, and therefore, the changes in the magnetic field configuration do not immediately affect the dust flow. For example, trajectory calculations indicate an approximately 6 year delay between solar magnetic field-reversals and the shift in the flow of ISD grains from focusing toward to defocusing away from the ecliptic plane (Sterken *et al.*, 2013). Ulysses measurements identified interstellar grains and determined their flow direction only by statistical means, and with large uncertainties. The full details of the influence of the heliosphere on the trajectories of ISD grains remains yet to be fully understood (Krüger and Grün, 2009).

Early dust instruments onboard Pioneer 8 and 9 and Helios spacecraft detected a flow of submicron-sized dust particles arriving from the solar direction. These particles originate in the inner solar system from comets, and from collisions among meteoroids, and move on hyperbolic orbits that leave the solar system under the prevailing radiation pressure force. The dust instrument onboard the Ulysses spacecraft observed escaping dust particles high above the solar poles, confirming the supposition that charged nanometer-sized dust grains are carried to high heliographic latitudes by electromagnetic interactions with the IMF. Recently, the STEREO WAVES instruments recorded a large number of intense voltage signals in the ecliptic plane at 1 AU, which were interpreted as impact ionization signals of streams of nanometer-sized particles striking the spacecraft at velocities of about solar-wind speed (Fig. 11.2). High fluxes of nanometer-sized dust grains at low heliographic latitudes, as well as strong spatial and temporal fluctuations of dust streams uncorrelated with solar-wind properties pose a mystery. The

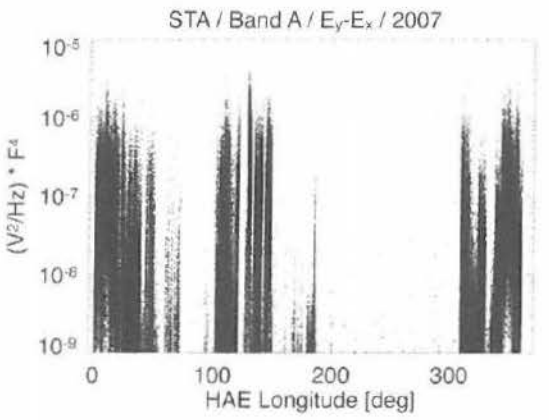

Fig. 11.2 The average power observed by the STEREO WAVES low-frequency receiver on STEREO A as a function of ecliptic longitude during 2007. The periods of high amplitudes have been suggested to be caused by high-speed nano-dust striking the spacecraft. (From Meyer-Vernet *et al.*, 2009.)

nano-dust, if real, represents a significant mass flux, which would require that the total collisional meteoroid debris inside 1 AU is cast in nanometer-sized fragments.

Dust adds mass to the solar wind as it is a source of atomic and molecular ions and neutrals, which are rapidly ionized. The charged ions and molecules are picked up by the solar wind magnetic field (Lemaire, 1990). However, the effects of mass loading by dust-generated species on the acceleration and dynamics of the solar wind near the Sun, including the position of the sonic point, where the subsonic solar wind plasma transitions to a supersonic flow, are not known and remain the subject of speculation. A slight increase in the average ion mass in the solar wind might, for example, generate shocks, at least in localized regions of high dust densities. These regions might also contribute to the energization of solar-wind ions via two-stream plasma instabilities (Shapiro *et al.*, 2005). Mass loading by dust has been invoked to explain enhancements observed in the IMF (Russell *et al.*, 1984). The exact nature, and the processes responsible for the generation of magnetic field enhancements remain an open issue.

Dust-generated neutrals and ions are thought to form an "inner source" of pickup ions (PUIs) whose velocity distribution differs from that of interstellar "outer source" PUIs. Both singly charged atomic ions and molecular ions (e.g., CH^+, NH^+, OH^+, and H_2O^+) have been identified in the inner source population (Gloeckler *et al.*, 2010). Processes proposed to explain the production of PUIs from the near-Sun dust include surface interactions and gas production by sublimation, sputtering, and collisional vaporization. Modeling indicates that collisional vaporization can account for the heavy elements in the inner source PUI population as well as molecular species, while surface interactions produce significant amounts of pickup protons (Mann and Czechowski, 2005). PUI production from dust sublimation or sputtering inside 0.1 AU is predicted to produce higher-charge-state PUIs; however, these processes have not yet been quantified (Mann, 2010). Solar-wind interaction with the near-Sun dust also contributes to the neutral solar wind and can generate energetic neutral atoms (ENAs) (Collier *et al.*, 2001) suggesting that dust interaction with solar energetic particles may be an additional inner heliospheric ENA source.

The dynamics of small charged dust particles in planetary magnetospheres can be surprisingly complex, possibly leading to levitation, rapid transport, energization and ejection, capture, and the formation of new planetary rings, for example. Dust particles immersed in plasmas are unusual charge carriers, and due to their very large mass compared to electrons and ions, they introduce new spatial and temporal scales. The Coulomb interaction between charged dust grains can lead to collective behavior, for example waves with unusually low frequencies and long wavelengths, making them visually observable in laboratory experiments. In this brief tutorial the discussion will be limited to dust charging, dust dynamics in

planetary magnetospheres and in interplanetary space, and possible dusty plasma collective effects at comets. The material discussed is based on a collection of review papers (Horányi, 1996; Horányi *et al.*, 2004, Mendis and Horányi, 2013a). Comprehensive reviews on many other aspects of the physics of dusty plasmas are also readily available (Bliokh *et al.*, 1995, Shukla and Mamun, 2002, Tsytovich *et al.*, 2010). In addition, several modern general plasma physics text books now include sections on dusty plasmas (Bellan, 2006, Piel, 2010).

11.2 Dust charging

If a dust grain carries a charge, its motion will be influenced by electromagnetic forces in addition to all other forces acting on uncharged dust particles. The relative importance of the electromagnetic forces due to either the large-scale electric and magnetic fields or small-scale fields between charged grains, depend on the charge-to-mass ratio of a dust particle. A single isolated dust grain embedded in a plasma with a Maxwellian energy distribution and shielded from any radiation field energetic enough to cause photoelectric emission from the grain, will acquire a negative average charge, if the ion and electron number densities ($n_e = n_i$) as well as the ion and electron temperatures ($T = T_e = T_i$) are equal. While this is rarely the case, the assumptions are used here to simplify our discussion below. The negative average charge is a consequence of the higher thermal speed of the electrons due to their much smaller mass. In equilibrium the surface potential ϕ (with respect to $\phi = 0$ at infinity), and the grain charge q_d, will be given by

$$\phi = \frac{q_d}{4\pi\varepsilon_0 r_d} = -\alpha\frac{k_B T}{e} \tag{11.1}$$

where ε_0 is the vacuum permittivity, r_d is the radius of the dust grain (which we will assume to be spherical, hence its capacitance $C = 4\pi\varepsilon_0 r_d^2$), and k_B is Boltzmann's constant (Spitzer, 1978). The proportionality factor α is a function of the ion mass m_i, and for example it is approximately 2.5, 3.6, and 3.9 for a pure H^+, O^+, and S^+ plasma, respectively. In equilibrium, the rate at which electrons collide with the grain is equal to the rate at which positive ions strike the grain if each ion is singly ionized.

In addition to the collection of electron and ion fluxes (that by themselves can be further complicated if a grain is embedded in a multi-species plasma with non-Maxwellian energy distributions), grains can charge due to a number of other processes, including photo, secondary, and thermionic emissions (see Fig. 11.3) (Whipple, 1981, Mendis, 2002, Horányi, 1996).

Naturally, a dust grain charge is in equilibrium if the sum of all the charging currents is zero. However, due to the stochastic nature of these charging currents

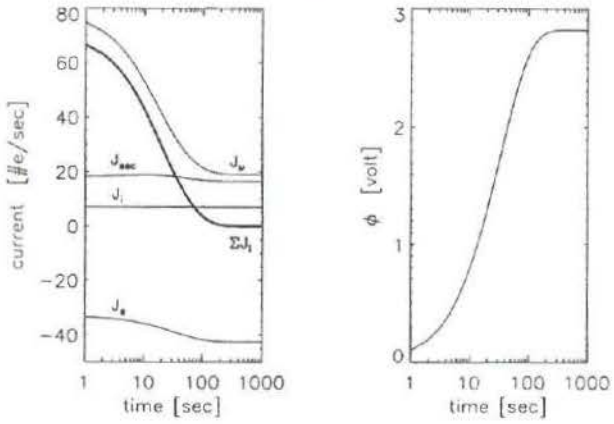

Fig. 11.3 The evolution of the electron and ion thermal currents, J_e, J_i; secondary and photoelectron currents J_{sec}, J_v, and their sum $\sum J_k$ (left panel); and the electrostatic surface potential ϕ (right panel) of an initially uncharged dust particle with radius $a = 1$ μm at a heliocentric distance of 1 AU. (From Horányi, 1996.)

the charge of any dust particle is expected to fluctuate around its equilibrium (Gail and Sedlmayr, 1975). The presence of neutrals can also influence the charging processes. In a weakly ionized plasma the electron and ion fluxes will be limited to diffusion currents. However, in the solar wind, or in magnetospheric plasma environments discussed in this tutorial, the standard plasma Langmuir probe equations (Langmuir, 1923) used in the calculations of these currents give satisfactory results for regions where the dust density is much smaller than the plasma density $n_d \ll n_p$.

In these cases dust grains can be treated as test particles and their distribution in space has a negligible effect on the electric, magnetic, and gravitational fields. Dust-particle trajectories can be followed by simultaneously integrating their time dependent charge, and the dynamical effects of gravitational, electric, and magnetic forces, drag, and radiation pressure (Horányi, 1996). Following a large number of single particle trajectories, the size and spatial distribution of these grains can be calculated, including possible time dependence in their production (micrometeoroid bombardment of moon sources) and loss (sputtering and collisions).

In regions where the dust density is no longer negligible compared to the plasma density, the charge of a grain can be greatly reduced compared to an isolated particle in the same plasma environment, due to the depletion of the plasma density (Goertz and Ip, 1984, Havnes, 1984, Whipple *et al.*, 1985).

The influence of dust on collective effects (i.e., waves and instabilities) is particularly strong in plasmas in which the dust carries a significant fraction of

either the negative or the positive charge. Havnes (1984) and Havnes *et al.* (1990) introduced the parameter

$$P \equiv \frac{4\pi\varepsilon_0 r_d}{e^2 n_0} n_{d0} k_B T \tag{11.2}$$

as an indicator of whether grains carry a significant fraction of the negative charge in a plasma in which photoelectric emission from the dust is unimportant. Here n_0 and n_{d0} are the number density of charges carried by ions and by dust, respectively. If $P \ll 1$, the dust will carry only a small fraction of the negative charge, and the magnitude of the average charge on a grain is well estimated by Eq. (11.1). If $P \gg 1$, the dust particles carry a large fraction of the negative charge and the average charge on a single dust particle is small compared to the result given by (11.1).

11.3 Dust in planetary magnetospheres

In order to follow the spatial and temporal evolution of dust density distributions in magnetized plasma environments, the equations describing the motion and the evolution of the charge of the particles have to be simultaneously integrated. The central body can be represented by multipole expansions of its gravitational and magnetic fields. The density and the temperature of the many-component plasma environment is to be predefined as a function of coordinates and, if necessary, the time as well. The charging currents are dependent not only on the instantaneous plasma parameters but on the velocity, as well as on the previous charging history of the dust grains. In Gaussian units the equation of motion of a dust particle with radius a, mass m, and charge Q, in an inertial coordinate system can be written as

$$\ddot{\mathbf{r}} = -\mu\nabla\left(\frac{1}{r} + \frac{R^2}{r^3}J_2P_2 + \frac{R^4}{r^5}J_4P_4\right) + \frac{Q}{m}\left(\frac{\dot{\mathbf{r}}}{c} \times \mathbf{B} + \mathbf{E}_c\right), \tag{11.3}$$

where $\mathbf{r}$ is the grain's position vector and an overdot signifies differentiation with respect to time. The first term on the right-hand side is the gravitational acceleration due to the planet with $\mu = GM$, the product of the gravitational constant G and the mass of the planet M, the planet's radius R, and the higher-order terms of its gravity are expressed in terms of Legendre polynomials P_2, and P_4 with coefficients J_2, and J_4, respectively, and possibly higher-order terms. The last term is the Lorentz acceleration where $\mathbf{B}$ is the local magnetic field and, assuming a rigidly co-rotating magnetosphere, the co-rotational electric field is

$$\mathbf{E}_c = (\mathbf{r} \times \boldsymbol{\Omega}) \times \mathbf{B}/c, \tag{11.4}$$

where $\boldsymbol{\Omega}$ is the angular velocity vector of the planet.

As grains traverse the various plasma regions their charge will not stay constant. A grain's charge can be followed via the current balance equation

$$\frac{dQ}{dt} = \sum_i I_i, \tag{11.5}$$

where I_i represent electron and ion thermal currents, and also the secondary and photoelectron emission currents. These are all functions of the plasma parameters, material properties, size, velocity, and also the instantaneous charge of a dust particle. This set of equations are already sufficient to find surprising outcomes: rapid dust transport, and even the energization and ejection of small grains from planetary magnetospheres.

11.3.1 Simplified dynamics

To gain insight into the dynamics of charged grains, we rewrite Eq. (11.3) for a grain moving in the equatorial plane of a spherical planet with a simple aligned and centered dipole magnetic field, using polar coordinates r, ϕ

$$\ddot{r} = r\dot{\phi}^2 + \frac{q}{r^2}(\dot{\phi} - \Omega) - \frac{\mu}{r^2} \tag{11.6}$$

$$\ddot{\phi} = -\frac{\dot{r}}{r}\left(\frac{q}{r^3} + 2\dot{\phi}\right). \tag{11.7}$$

We introduced $q = QB_0R^3/(mc)$, where B_0 is the magnetic field on the surface of the planet on its equator, and the combination $q/r^3 = \omega_g$, becomes the gyrofrequency of the dust particle (i.e., the angular rate the dust particle circles about magnetic field lines).

On a circular equilibrium orbit $\ddot{\phi} = \ddot{r} = \dot{r} = 0$, and $\dot{\phi} = \text{constant} = \psi$. The differential equations in this case turn into an algebraic equation for the angular velocity ψ

$$\psi^2 + \omega_g\psi - \omega_g\Omega - \omega_K^2 = 0, \tag{11.8}$$

where $\omega_K = (\mu/r^3)^{1/2}$ is the Kepler angular rate of an uncharged particle on a circular orbit at a distance r from the planet. For big particles, terms that contain ω_g can be dropped and we recover $\psi = \pm\omega_K$, prograde or retrograde Kepler orbits. For very small particles, terms that are not multiplied with ω_g are to be dropped and $\psi = \Omega$. Very small grains are picked up by the magnetic field and co-rotate with the planet. These differential equations can be integrated to yield constants of the motion

$$\mathcal{E} = \frac{1}{2}(\dot{r}^2 + r^2\dot{\phi}^2) = \frac{\mu + q\Omega}{r}, \tag{11.9}$$

$$\mathcal{J} = r^2\dot{\phi} - \frac{q}{r}. \tag{11.10}$$

For large particles ($q \to 0$) these constants become the Kepler energy and angular momentum. The Jacobi constant, $\mathcal{H} = \mathcal{E} - \Omega\mathcal{J}$, remains a constant even if q changes with time (Northrop and Hill, 1983). For a fixed $\mathcal{J}$ the effective 1D potential (i.e., $\ddot{r} = -\partial U/\partial r$) becomes

$$U(r) = -\frac{\mu + q\Omega}{r} + \frac{\mathcal{J}^2}{2r^2} + \frac{q\mathcal{J}}{r^3} + \frac{q^2}{2r^4}. \tag{11.11}$$

Small dust particles are generated by interplanetary dust particle impacts, or by active volcanoes and plumes. In these cases the small particles have initial relative speeds that are small compared to the orbital speed of their parent body. For an initial Kepler orbit $\mathcal{J} = r^2(\omega_K - \omega_g)$. Figure 11.4 shows $U(r)$ for particles originating from Io ($r_0 = 5.9\ RJ$) at Jupiter for the two typical values -30 and $+3$ V for the surface potential $\phi = Q/a$ (Horányi *et al.*, 1993a,b). Particles with negative surface potentials remain confined in the vicinity of r_0. However, grains in a certain size range with positive charges are not confined as $U(r)$ shows no minima. In the case of positively charged grains the force due to the co-rotational electric field points radially out, opposing gravity. The upper limit in size for ejection a_{max}, is set by the condition $F_E/F_G > 1$. The lower limit in dust size for ejection results from the fact that very small grains behave like ions or electrons circling magnetic field lines. The gyroradius $r_g = |wmc/(QB)| = |w/\omega_g|$, where

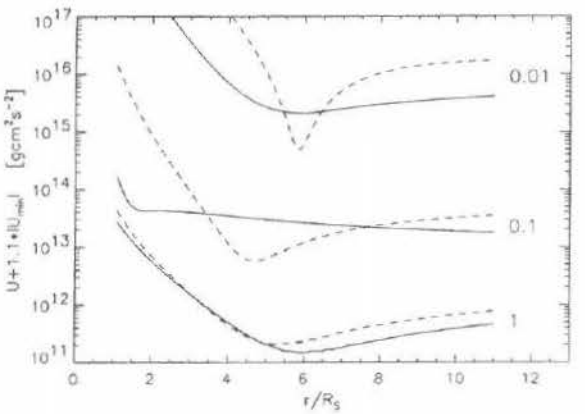

Fig. 11.4 The effective potential for dust grains with $a = 0.01, 0.1$, and $1\ \mu$m started from Io on circular Kepler orbits with $\phi = -30$ (dashed lines) and $+3$ V (continuous lines). To avoid the overlap of these curves, because only their shape is important, we have shifted them apart by plotting $U + 1.1|\text{minimum}(U)|$ instead of U itself. (From Horányi, 1996.)

w is the relative velocity between the co-rotating magnetic fields and the particle. For Kepler initial conditions $w = r(\Omega - \omega_K)$. The motion of these grains is well described by the guiding center approximation if the size of their orbit is smaller than the characteristic length scale for variations in the magnetic fields, $|r_g \nabla B/B| < 0.1$ ($|\nabla B/B| = 3/r$ in the equatorial plane of an aligned centered dipole). The upper limit of grain size satisfying this condition (i.e. the smallest grains that will be ejected) is

$$a^* \, [\mu\text{m}] = \left(\frac{10^{-3} B_0 R^3 \phi}{4\pi r^2 \rho \omega c} \right)^{1/2}. \tag{11.12}$$

Grains in the size range $a^* < a < a_{max}$ will be ejected from the magnetosphere. As these positively charged grains move outward they gain energy from the co-rotational electric field

$$W = \int_{r_0}^{r_1} EQdr = E_0 R^2 Q \left(\frac{1}{r_0} - \frac{1}{r_1} \right), \tag{11.13}$$

where the upper limit of the integration, r_1, is the characteristic size of the magnetosphere. This mechanism was suggested to explain the Ulysses and Galileo observations at Jupiter (Horányi *et al.*, 1993a,b) and the Cassini measurements at Saturn (Horányi, 2000; Kempf *et al.*, 2005) of small dust grains streaming away from these planets.

11.3.2 Stream particles at Jupiter and Saturn

Small grains ejected from planetary magnetospheres represent a surprising example of the possible complexity of the dynamics of charged dust particles. Electrons and ions with their large charge-to-mass ratios follow adiabatic motion and remain confined by magnetic fields. Large dust particles with vanishingly small charge-to-mass ratios follow Kepler orbits and remain bound by gravity. When the magnitude of the electromagnetic and gravitational forces are comparable the outcome can be quite surprising.

Jupiter was first recognized as a source of dust particles during Ulysses' encounter with the planet in 1992, as high speed intermittent streams of small grains were discovered (Grün *et al.*, 1993). The first estimates put the mass of the stream particles in the range of $1.6 \times 10^{-16} < m < 1.1 \times 10^{-14}$ g and their velocity in the range of $20 < v < 56$ km/s. Assuming an average density $\rho \simeq 1$ g cm^{-3}, the radii of these grains were estimated in the range of $0.03 < a < 0.1$ μm. However, these estimates remained uncertain, because the detector was not calibrated in this size and velocity range. Similar fluxes were seen with the identical dust detector onboard the Galileo spacecraft as it first approached Jupiter in 1995 (Grün *et al.*,

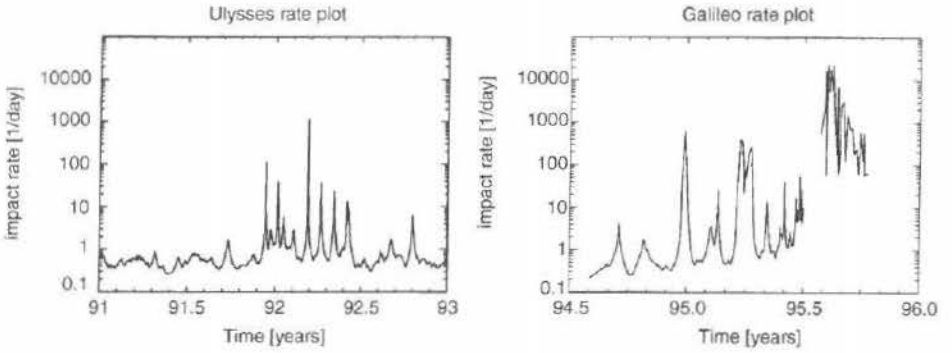

Fig. 11.5 Dust impact rates measured by *Ulysses* (left) and by *Galileo* (right) at Jupiter. (From Horányi, 1996.)

1997). The discovery observation from Ulysses and the data from Galileo's initial approach to Jupiter are shown in Fig. 11.5.

High-velocity streams of nanometer-sized dust particles originating from the inner Saturnian system were observed during Cassini's approach to Saturn (Kempf *et al.*, 2005, Hsu *et al.*, 2010). The Cosmic Dust Analyzer (CDA) often registered impact signals that were most likely caused by particles moving faster than 70 km/s, the fastest impact speed for which CDA was calibrated at the Heidelberg dust accelerator facility. Using Eq. (11.13) to calculate the work done by the co-rotating electric field and the expected charges of the grains, a simple order-of-magnitude relationship can be derived to show that the expected escape velocity is inversely proportional to the size of the particles (Horányi and Juhász, 2000):

$$v_{escape} = \frac{3}{a\,[\mu\mathrm{m}]}\ \mathrm{km/s} \quad \text{for Jupiter, and} \tag{11.14}$$

$$v_{escape} = \frac{0.6}{a\,[\mu\mathrm{m}]}\ \mathrm{km/s} \quad \text{for Saturn.} \tag{11.15}$$

These expressions assume that Jovian dust particles start at Io, and that Saturn's grains are accelerated outward from Dione's distance, because that is where the grains' charge becomes positive in Saturn's magnetosphere. The faster speeds at Jupiter result mainly from its stronger magnetic field. Beyond Saturn's magnetosphere, the dynamics of the stream particles is governed by interactions with the interplanetary magnetic field convected by the solar wind.

11.3.3 Spokes in Saturn's rings

Spokes are intermittently appearing, approximately radial markings on Saturn's B ring (Fig. 11.6), consisting of small charged dust particles lofted from their parent

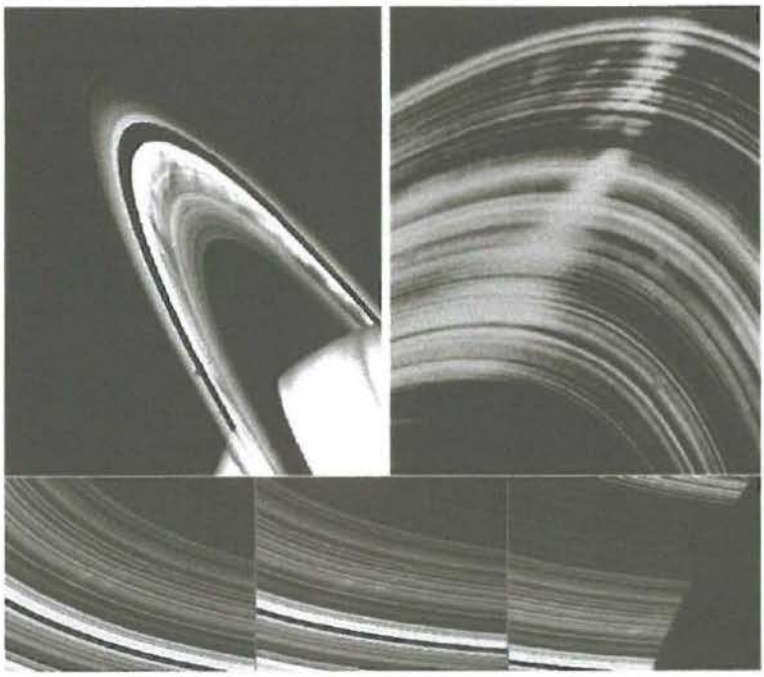

Fig. 11.6 Top: spokes in the B ring as seen by Voyager 2 (Smith *et al.*, 1982). The left-hand image was captured in back-scattered light before closest encounter, with the spokes appearing as dark radial features across the ring's center. The right-hand image was taken in forward-scattered light after the spacecraft crossed the ring plane, and was looking back towards the Sun; the spokes now occur as bright markings. Typical dimensions of these spokes are 10 000 km in length and 2000 km in width. The nature of the changing brightness indicates that spokes consist of small submicron-sized grains, i.e., that are comparable in size to the wavelength of visible light. At the time these images were taken, the rings' opening angle to the Sun was $B_0 \simeq 8°$. Bottom: the initial spoke observations taken by Cassini on September 5, 2005 ($B_0 \simeq 20°$), over a span of 27 min. These faint and narrow spokes were seen from the un-illuminated side of the B ring. These first spokes are $\simeq$ 3500 km long and 100 km wide, smaller than the average spokes seen by Voyager. These images were taken with a resolution of 17 km per pixel at a phase angle of 145° when Cassini was 135° above the unlit side of the rings as the spokes were about to enter Saturn's shadow (Mitchell *et al.*, 2006).

ring bodies owing to electrostatic repulsion. While they were first recognized in images taken by Voyagers 1 and 2 (Smith *et al.*, 1981, 1982), spokes were possibly noticed even earlier in ground-based telescopic observations (Robinson, 1980). These perplexing features have attracted great attention; following their appearance in Voyager 1 images, Voyager 2, during its approach to Saturn, dedicated sequences to spoke observations, providing an invaluable dataset. The spokes' characteristics have been derived with an increasing level of sophistication since

their acquisition in these images. The desire to provide an explanation for the spokes has played a large role in the emergence of the research field of Dusty Plasmas.

The key physical characteristics of spokes based on the Voyager (Porco and Danielson, 1982; Grun *et al.*, 1983; Grün *et al.*, 1992; Eplee and Smith, 1984; Doyle and Grun, 1990) and Cassini (Mitchell *et al.*, 2013) data can be summarized as follows: These features are generally most common near the morning terminator, (i.e., the ring extremity (or ansa) on the dawn side), and seem to form primarily in that region. Spokes develop on a time scale of minutes, and can become more intense over a period of a few hours. Appearing at radial distances that are near to, or straddle, synchronous orbit, they move around the ring nearly co-rotating with the planet. During increases in spoke intensity, these features extend forwards and backwards from the synchronously moving longitude inside and outside the co-rotation distance, respectively, while their central regions intensify; this indicates that the spoke material follows Keplerian trajectories, in broad terms at least. Once spokes no longer intensify, they fade while traveling around the dayside of the rings. Newly formed spokes in the Voyager data often coincided with the positions of older spokes that seem to have survived an entire revolution around Saturn. The periodicity of spoke formation is close to the observed period of a strong low-frequency radio emission, called the Saturn kilometric radiation (SKR) measured by the Voyagers (Porco and Danielson, 1982), suggesting a formation trigger that is linked to Saturn's magnetic field.

Numerous formation theories were proposed to explain the spokes' existence, but none could be definitively tested without further observations. The Hubble Space Telescope (HST) monitored spoke activity from 1995 until 1998, when HST no longer detected spokes due to Saturn's equinox (when the solar illumination hit the rings edge-on). McGhee *et al.* (2005) proposed that spokes, while always present, can be detectable only when the observer lay close to the ring plane. It was therefore anticipated that Cassini would detect spokes on its 2004 arrival at Saturn and that its observations would finally decide which, if any, of the competing theories were correct (Horányi *et al.*, 2004). However, contrary to predictions, Cassini did not observe spokes, even when close to the ring plane, until September 2005 (Fig. 11.6). The variability in spoke occurrence in HST data was therefore not an observational effect: spokes are indeed a seasonal phenomenon, and their formation can be suspended for extended periods. This seasonal variation of spoke activity may be a consequence of the variable plasma density near the ring. The plasma density is a function of the solar elevation angle $B_{\odot}$, measured from the ring plane, because it is generated mainly from the rings by photoelectron production and by photo-sputtering of neutrals that are subsequently ionized (Mitchell *et al.*, 2006; Farrell *et al.*, 2006).

Spokes are comprised of dust particles in a narrow size distribution centered at about a radius $s \simeq 0.6$ μm (Doyle and Grun, 1990). It is generally believed that spoke formation involves charging and thus electric fields acting on these small grains, but this process requires, as we show below, a much higher plasma density than is commonly expected near the rings (Hill and Mendis, 1982; Goertz and Morfill, 1983). When formed, spokes initially cover an approximately radial strip with an area of $A \simeq 10^3 \times 10^4$ km^2, with a characteristic optical depth of $\tau \simeq 0.01$. The total number of elevated grains can be estimated to be on the order of $N_d \simeq A\tau/(\pi s^2) \simeq 10^{23}$. If the grains are released approximately at the same time and carry just a single electron when released from their parent bodies, the formation of the spoke cloud requires a minimum surface charge density (measured in units of electron charges e) $\sigma_e^* = N_d/A \simeq 10^6$ cm^{-2}, orders of magnitude higher than the charge density, σ_0, expected from the nominal plasma conditions in the B ring.

The nominal plasma environment near the optically thick B ring is set by the competing electron and ion fluxes to and from the ring due to photoelectron production from the ring (as well as the ionosphere) and the photoionization of the rings' neutral atmosphere that is maintained by photo-sputtering. All of these are expected to show a seasonal modulation with the ring's opening angle with respect to the Sun, $B_\odot$. The characteristic energy for photoelectrons is $T_e \simeq 2$ eV, and the plasma density is expected to be $n \sim 0.1$–1 cm^3 (Waite *et al.*, 2005). The characteristic plasma shielding distance is $\lambda_D = 740 \times (T_e/n)^{1/2} \simeq 1$–$3 \times 10^3$ cm, larger than the average distance between the cm–m sized objects in the B ring, which has a comparable vertical thickness, $h \simeq 10$ m. Hence, it is reasonable to treat the B ring as a simple sheet of material (Goertz and Morfill, 1983). The nominal surface potential, including its possible seasonal variations, is expected to be in the range of $-5 < \phi_R < 5$ V. The surface charge density can be estimated from Gauss's law,

$$\sigma_0 \simeq \frac{\phi_R}{4\pi\lambda_D} \simeq 2.5\phi_R \left(\frac{m}{T_e}\right)^{1/2} < 1\text{–}3 \times 10^3 \text{cm}^{-2}. \tag{11.16}$$

Because $\sigma_0 \ll \sigma_e^*$, the formation of a spoke requires higher than normal plasma densities.

Several spoke formation theories have been put forward (McGhee *et al.*, 2005). Of these, the proposed spoke formation trigger theories that arguably have been most widely accepted are those of meteoroid impacts onto the rings (Goertz and Morfill, 1983) and field-aligned electron beams originating from the auroral regions of Saturn (Hill and Mendis, 1982). Both of these could transiently increase the plasma density above a critical threshold, and trigger the formation of spokes.

A meteoroid impact-produced plasma cloud was shown to expand, cool and recombine as it rapidly propagates in the radial direction, possibly explaining many

of the observed spoke characteristics (Goertz and Morfill, 1983). However, the estimated propagation speed of such a cloud remains difficult to estimate (Farmer and Goldreich, 2005; Morfill and Thomas, 2005). The electron-beam mechanism has been suggested to loft small particles instantaneously along the entire radial extent of a spoke (Hill and Mendis, 1982). Other spoke formation ideas include dusty plasma waves (Tagger *et al.*, 1991; Yaroshenko *et al.*, 2008) and impact-induced avalanches of small charged dust particles (Hamilton, 2006).

During the first four years (2004–2008) of Cassini observations spokes remained a high priority. For most of this interval, spokes were much fainter and less frequent than those seen by the Voyagers. By late 2008, $B_{\odot}$ had reached values similar to those during the Voyager encounters, and spoke activity was indeed approaching – if not matching – the activity observed by the Voyagers (Mitchell *et al.*, 2008). Based on the increase in spokes at the time of writing, it is anticipated that Cassini should answer key questions regarding the nature of these perplexing ring features by the end of its mission in 2017.

11.4 Waves in dusty plasmas: possible role in comets

The presence of charged dust can alter collective behavior of the plasma as manifested by altered dispersion relationships of the customary plasma waves, and the emergence of new plasma waves and instabilities (Shukla and Mamun, 2002; Bliokh *et al.*, 1995; Tsytovich *et al.*, 2010). In the following we describe dusty plasma wave modes that possibly have relevance to comets.

The so-called "Dust Ion Acoustic" (DIA) dusty plasma wave was predicted by Shukla and Silin (1992) and it was first observed in the laboratory by Barkan *et al.* (1996). Here the charged dust does not participate in the wave dynamics; it simply modifies the wave mode via the quasi-neutrality condition in the plasma. If we consider the simple case of dust particles (all of the same size) in a singly ionized two-component (electron and ion) thermal plasma, where the only charging currents to the grains are electron and ion collection, the grains become negatively charged (as discussed in Sect. 11.2). If each dust grain carries an excess of Z electrons on its surface, the quasi-neutrality condition in the undisturbed plasma is:

$$n_{i0} = n_{e0} + Zn_{d0}, \tag{11.17}$$

where $n_{\alpha 0}$ refers to the ion, electron, and dust number densities in the undisturbed plasma. Note that this leads to a depletion in the electron density relative to the ion density. This increases the phase velocity of a DIA wave above the usual ion acoustic wave in a dust-free plasma. With the approximation of negligible electron inertia and immobile dust grains, the dispersion relation for the DIA wave is given by (Shukla and Silin, 1992)

$$\omega^2 = \frac{\delta k^2 c_s^2}{1 + k^2 \lambda_{De}^2}, \tag{11.18}$$

where $c_s = (k_B T_e / m_i)^{1/2}$ is the usual ion acoustic speed, λ_{De} is electron Debye shielding length, and $\delta = (n_{i0}/n_{e0})$. Hence, in a dust-free charge-neutral plasma $\delta = 1$, and the DIA dispersion relationship is simply that of an ion-acoustic wave (Chen, 1974). In the long-wavelength regime ($k\lambda_{De} \ll 1$), Eq. (11.18) reduces to

$$\omega = k\delta^{1/2} c_s. \tag{11.19}$$

Because $\delta^{1/2}$ could be $\gg 1$ if the electron depletion due to dust is sufficiently large, the phase velocity (ω/k) of this wave could be $\gg c_s$, and, consequently, Landau damping could become negligible. This is in contrast to a pure electron–ion plasma, where $T_e \gg T_i$ is required for the acoustic wave to remain undamped. The implication of this in various cosmic dusty plasma environments was discussed by Mendis and Rosenberg (1994).

Several authors have considered the excitation of the dust ion acoustic instability in the Saturnian magnetosphere, due to the relative motion of the co-rotating plasma and the charged dust particles moving with speeds intermediate between co-rotation and the local Kepler velocity (Rosenberg, 1993; Winske *et al.*, 1995). Both the linear and the non-linear properties of this instability have been investigated, including its saturation due to the trapping of plasma ions. It has been identified as a possible explanation for the temperature increase of O^+ ions in the region 4–8 R_S from about 40 to 200 eV, first observed by the Voyager mission at Saturn (Richardson and Sittler, 1990). There is also relative motion between the charged dust and the plasma throughout the cometary dusty plasma environment, in both the cometary head and the tail. Perhaps, a good candidate location is the region behind the nucleus where the already high-speed ions forming the ion tail diverge from the flow of dust into the dust tail of a comet.

The second dusty plasma wave mode to consider is the so-called "Dust Acoustic" (DA) mode, whose existence was predicted by Rao *et al.* (1990), and confirmed in the laboratory by Barkan *et al.* (1995). In this case, contrary to the DIA mode, the charged dust grains also participate in the wave dynamics, in addition to modifying the usual quasi-neutrality condition. The laboratory experiment, shown in Fig. 11.7, used a potassium plasma with $k_B T_e \simeq 3$ eV, $k_B T_i \simeq 0.2$ eV, micron-sized dust grains of equal mass $m \simeq 10^{-15}$ kg, a typical dust charge of $Z_d \simeq 2 \times 10^3$e, and had $n_d/n_i \simeq 5 \times 10^{-4}$. In this setup a slowly propagating ($v_\varphi \simeq 9$ cm/s), long-wavelength ($\lambda \simeq 0.6$ cm), low-frequency ($\omega \simeq 15$ Hz), longitudinal wave of significant amplitude ($A = |\Delta n_d / n_{d0}| \simeq 1$) was observed by laser scattering. With these conditions (i.e., $k_B T_e \gg k T_i$), in the long-wavelength regime ($k\lambda_{De} \ll 1$) the dispersion relation of the DA mode reduces to (Rao *et al.*, 1990)

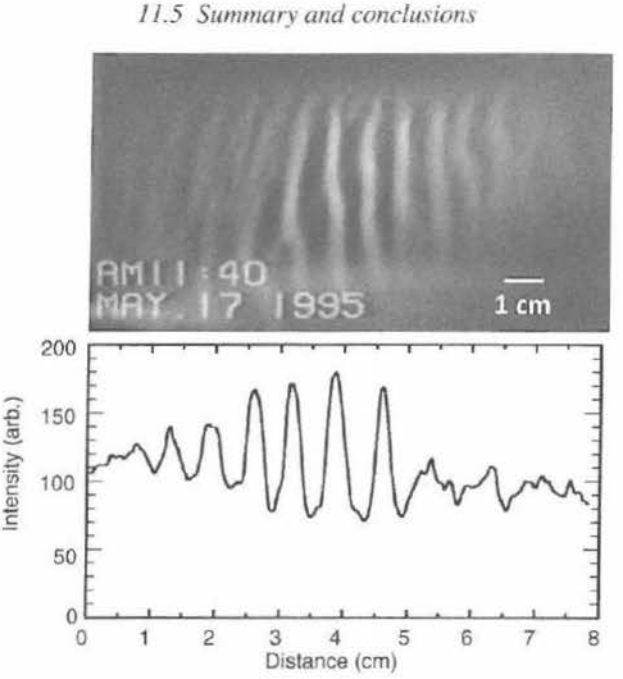

Fig. 11.7 Single video frame image of a Dust Acoustic Wave (DAW) observed in the laboratory. The bright vertical bands correspond to the wave crests (dust compressions). The wavelength can be seen to be $\lambda \simeq 0.6$ cm. By following the wave fronts from frame to frame of the video, the wave speed was measured $v_\varphi \simeq 9$ cm/s, so that the frequency $f = v_\varphi/\lambda \simeq 15$ Hz (Thompson *et al.*, 1999).

$$\omega^2 = Z_d^2 k^2 \left(\frac{k_B T_i}{m_d} \frac{n_{d0}}{n_{i0}} \right). \tag{11.20}$$

Substituting the experimental values in Eq. (11.20) $v_\varphi = \omega/k \simeq 10$ cm/s, results in a good agreement with the observed value.

The possibility of observing such waves in the dusty plasma environment of comets has not been discussed in the literature, and owing to their small spatial scales, could not have been possibly observed during the fly-by missions to date. The high-resolution cameras onboard Rosetta might be able to capture the propagating small-scale structures of possible DA waves. Perhaps, new dusty plasma phenomena will be found by Rosetta that could lead to the inference of the excitation of DIA and DA waves and instabilities (Mendis and Horányi, 2013a,b).

11.5 Summary and conclusions

In most solar-system plasma environments the dynamics of small charged particles is strongly influenced, if not dominated, by electromagnetic forces acting

simultaneously with gravity, drag, and radiation pressure. Dust particles traversing various regimes adjust their electrostatic charges as dictated by the changing plasma conditions, and in fact they act as active electrostatic probes, continuously adjusting their surface potential towards the local equilibrium value. The fields and particle environment can uniquely shape the size and the spatial distribution of the dust grains. Dust particles are unusual charge carriers, as compared to electron or ions, as their charge-to-mass ratio is not fixed. Micron-sized dust particles can have thousands of missing or extra electrons. Because of their huge mass, they enable physical processes on very different spatial and temporal scales compared to plasmas composed of electrons and ions only. Dusty plasma waves, for example, can show wavelengths and frequencies that enable them to be visually observed and easily recognized.

Studies of the motion of charged dust particles connect a number of observations that are often thought to be unrelated. Space missions, in general, are designed to make simultaneous in-situ and remote observations with some combination of the following experiments.

- New sophisticated dust detectors (Grün *et al.*, 2003, Fiege *et al.*, 2014) can provide in-situ measurements of the mass, velocity vector, charge, chemical, and possibly even the isotopic composition of the dust grains.
- Plasma instruments provide the composition, density, and energy distributions of the electrons and ions. These data are used to calculate the charging currents of the grains and to learn whether grains are in charge equilibrium or will have significant charge variations due to fluctuations and/or gradients in composition and/or density and/or temperature of the plasma. Apparent lack of charge balance between electrons and ions can result from the presence of sufficiently large dust densities (Ye *et al.*, 2014b; Morooka *et al.*, 2011).
- The plasma-wave and radio-science experiments onboard Voyager detected broad-band noise passing through the ring planes at Saturn, Uranus, and Neptune. This noise is believed to be caused by small dust grains bombarding the body of the spacecraft. The few kilometer per second relative velocity between the spacecraft and the dust grains is sufficient to fully vaporize the impacting grains and in part ionize the produced gas. The expanding plasma cloud causes the detected noise. This phenomenon led to the recognition that all giant planets are surrounded by vast tenuous sheets of small grains that could not have been discovered via imaging alone (Gurnett *et al.*, 1983; Ye *et al.*, 2014a).
- A magnetometer provides in-situ field measurements that can be used to describe the global structure of magnetic fields (Behannon *et al.*, 1977; Dougherty *et al.*, 2004). These data are essential to calculate the trajectories of charged dust particles.

- An imaging experiment can supply images taken through filters at various phase angles to show the spatial and size distribution of the dust particles. Ultimately, the spatial distributions of the fine dust can be independently modeled based on the transport processes at work and compared with the images (Juhász *et al.*, 2007).

It is a unique and powerful consistency test if our models describing dust transport, based on particles and field data, match the observations of the dust detectors and the images. However, without in-situ data on particles and fields, images showing the spatial distribution of small dust grains can be used to infer the plasma conditions. In addition to planetary magnetospheres and comets included in this tutorial, there are many other examples where dust and plasma interactions might be important. These include the propagation of interstellar dust particles through the heliosphere, noctilucent clouds in the Earth's mesosphere, or the surfaces of all airless planetary bodies.